Physics of Plasmas

Generation of forerunner electron beam during interaction of ion beam pulse with plasma

Cite as: Phys. Plasmas **25**, 011609 (2018); https://doi.org/10.1063/1.5002688
Submitted: 31 August 2017 . Accepted: 18 December 2017 . Published Online: 10 January 2018

Kentaro Hara, Igor D. Kaganovich, and Edward A. Startsev

COLLECTIONS

Paper published as part of the special topic on Collective Effects in Particle Beams and Nonneutral Plasmas; in Honor of the Late Prof. Ron Davidson

ARTICLES YOU MAY BE INTERESTED IN

Amplification due to two-stream instability of self-electric and magnetic fields of an ion beam propagating in background plasma
Physics of Plasmas **25**, 052122 (2018); https://doi.org/10.1063/1.5038878

Nonlinear structures and anomalous transport in partially magnetized $E \times B$ plasmas
Physics of Plasmas **25**, 011608 (2018); https://doi.org/10.1063/1.5001206

Electrostatic solitary waves in ion beam neutralization
Physics of Plasmas **26**, 050704 (2019); https://doi.org/10.1063/1.5093760

PHYSICS OF PLASMAS 25, 011609 (2018)

Generation of forerunner electron beam during interaction of ion beam pulse with plasma

Kentaro Hara,[1,2,a)] Igor D. Kaganovich,[2,b)] and Edward A. Startsev[2]
[1]*Department of Aerospace Engineering, Texas A&M University, College Station, Texas 77843-3141, USA*
[2]*Princeton Plasma Physics Laboratory, Princeton University, Princeton, New Jersey 08543, USA*

(Received 31 August 2017; accepted 18 December 2017; published online 10 January 2018)

The long-time evolution of the two-stream instability of a cold tenuous ion beam pulse propagating through the background plasma with density much higher than the ion beam density is investigated using a large-scale one-dimensional electrostatic kinetic simulation. The three stages of the instability are investigated in detail. After the initial linear growth and saturation by the electron trapping, a portion of the initially trapped electrons becomes detrapped and moves ahead of the ion beam pulse forming a forerunner electron beam, which causes a secondary two-stream instability that preheats the upstream plasma electrons. Consequently, the self-consistent nonlinear-driven turbulent state is set up at the head of the ion beam pulse with the saturated plasma wave sustained by the influx of the cold electrons from upstream of the beam that lasts until the final stage when the beam ions become trapped by the plasma wave. The beam ion trapping leads to the nonlinear heating of the beam ions that eventually extinguishes the instability. *Published by AIP Publishing.*
https://doi.org/10.1063/1.5002688

I. INTRODUCTION

The two-stream instability plays an important role in fusion,[1–4] astrophysics,[5–8] electrostatic shocks,[9,10] double layer formation,[11,12] and thrusters.[13] In particular, nonrelativistic ion beams can be used for heavy ion fusion and warm-dense matter experiments.[14–16] Neutralization of the ion beam is particularly important for the beam quality as the space charge may defocus the beam,[17–20] which has been studied for under-dense[19] and tenuous[21] plasmas. Longitudinal[22,23] and transverse compression[24–27] have also been investigated to increase the ion beam density.

A neutralized ion beam triggers an electrostatic two-stream instability between beam ions and plasma electrons; the instability saturates due to wave-particle trapping of either beam ions or plasma electrons.[23] Some fraction of the wave-trapped electrons becomes detrapped and streams ahead of the neutralized ion beam pulse. This results in generation of a beam of accelerated electrons, which we call forerunner electrons. Similarly, such electron acceleration is observed in electrostatic shocks.[28] As a consequence, a secondary two-stream instability develops between the forerunner and background electrons. Although forerunner electrons due to two-stream instability have been observed for collisionless shocks,[28] the mechanism of forerunner electron beam generation for the tenuous ion beam pulse propagating in a dense plasma is different from collisionless shocks. In collisionless shocks, forerunner electron beam generation occurs due to fast thermalization in electron-electron interaction, where the two-stream instability quickly mixes two electron streams and generates accelerated electrons in this rapid process. We consider a different process—the electron thermalization by a tenuous ion beam pulse. This process occurs in three stages and is sufficiently different from the process in collisionless shocks. In a typical laminar double layer structure formed by a low-Mach number electrostatic shock, accelerated electrons are not formed.[10,29] This indicates that a dynamic process is required to perturb the plasma electrons to travel ahead of the structure (e.g., beam, shock, etc.).

It is important to investigate the long-time evolution of the interaction between the ion beam and background plasma, mainly whether the secondary instability induced by the forerunner electrons affects the ion beam ballistic propagation. The saturation of the initial two-stream instability by wave trapping has been investigated in Refs. 23 and 27, where a small computational domain around the beam pulse was used to perform two-dimensional simulations. Nonetheless, the effects of the forerunner electrons (i.e., electron acceleration and wave decay processes) were not thoroughly investigated. Recent simulations show that large spatial domain and long temporal simulations are essential to investigating the long-time dynamics of the beam-plasma interactions.[30,31]

The focus of this paper is to study the later phase of the two-stream instability—(i) how the electrons become detrapped from the plasma wave and accelerate ahead of the ion beam pulse and (ii) how they affect long-time evolution of the initial two-stream instability. Therefore, we report the results of a large-scale, one-dimensional electrostatic kinetic simulation of the interaction between the ion beam pulse and background plasma.

II. KINETIC SIMULATION

Electrostatic kinetic simulations are performed in the frame of the ion beam. A standard particle-in-cell (PIC) simulation[32] is used for the ion beam pulse, background ions, and background electrons. The cell size is $\Delta x = L/N_x$, where $L = 15$ m is the domain length and $N_x = 3 \times 10^4$ is the number

[a)]Electronic mail: khara@tamu.edu
[b)]Electronic mail: ikaganov@pppl.gov

of cells. Li^+ is assumed for the ions. The electron temperature is 0.4 eV; the ion temperature is 0.3 eV; and the ion beam temperature is 0 eV. The ion beam density profile is assumed to be a Gaussian pulse with a duration of 20 ns. The plasma density is $n_p = 5.5 \times 10^{16}\,\mathrm{m}^{-3}$, the ion beam density is $n_b = 2 \times 10^{15}\,\mathrm{m}^{-3}$, and the ion beam velocity is chosen to be $v_b = c/30$, where c is the speed of light; the beam and plasma parameters are similar to the neutralized drift compression experiment (NDCX) parameters.[27] Such ion beam energy is also observed in proton beam generation by ultraintense lasers[33] and in collisionless shock.[34] The boundary conditions for the Poisson equation are $\phi = 0$ and $\partial_x \phi = 0$ at the boundary in front of the beam. The presented results are checked for convergence using small grid sizes (0.1 mm) and a large number of computational particles (3000 particles per cell), as well as with a separate Vlasov simulation solver[35,36] with comparable grid sizes in phase space.

III. RESULTS

After the beam is injected into a plasma, the two-stream instability develops and saturates nonlinearly. The linear growth and nonlinear saturation of the instability are investigated in detail.

A. Multiple stages of the two-stream instability

Several stages of evolution of the two-stream instability between the beam ions and plasma electrons can be observed in Fig. 1. We focus on nonlinear stages of the instability 200 ns after injection into a plasma, when we initialize time $t = 0$ ns presented in all figures. At $t \leq 0$ ns, the potential modulations are relatively small and confined to the beam pulse region ($|x - v_b t| < 10$ cm). The phase velocity of plasma wave and the wavelength of the modulation agree with theoretical predictions:[37] $v_\phi - v_b = -(\gamma/\sqrt{3})/k = -5.6 \times 10^4$ and $l = 2\pi/k = 2\pi v_b/\omega_{pe} \approx 4.8$ mm, where $\gamma/\omega_{pe} \approx (\sqrt{3}/2)\sqrt[3]{n_b/n_p \cdot m_e/m_{i,b}}$ is the growth rate of the ion-beam induced two-stream instability and $\omega_{pe} = \sqrt{4\pi e^2 n_p/m_e}$ (e, m_e, and $m_{i,b}$ being the electric charge, electron mass, and beam ion mass). The potential amplitude grows until saturation due to electron trapping.[38]

Electron trapping can be clearly observed in plasma electron phase plots shown in Fig. 1(b), where the electron velocity modulation reaches levels of ion beam velocity, v_b. It can be seen at $t < 0$ ns that the potential amplitude is less than $2\phi_0$, where ϕ_0 is the amplitude required for electrons to be trapped around $v = v_b$. Here, $\phi_0 = \frac{1}{2} m_e v_b^2 \approx 287$ eV. As the potential amplitude becomes larger and the wave is no longer single mode, the forerunner electrons form around $t = 0$ ns. The plasma potential at the tail of the beam ($x - v_b t < 0$) is positive with respect to the head of the ion beam ($x - v_b t > 0$). Reflection of plasma electrons will only occur if there is a negative potential, of which the amplitude is larger than ϕ_0. *Such a potential structure is not formed and the forerunner electrons are not caused merely by reflection from a potential hill*. Note that the potential hill observed in the simulation will result in electron acceleration toward the tail, not reflection. The reason for such potential hill formation is to prevent average background electron acceleration (in the laboratory frame) due to the ponderomotive force. Because in one-dimensional systems, the total current is conserved and electron current generated due to ponderomotive force would be higher than the ion beam current,[23,24] an average electric field is generated to prevent such electron acceleration as evident in Fig. 1(a). Because for the considered beam and plasma parameters at saturation $eE/m\omega_{pe} \sim v_b$, such generated potential is of order of ϕ_0. Figure 1(c) shows the ion beam phase space during the two-stream instability. It can be seen that the two-stream instability is most intense first at the tail of the ion beam. Hence, the electron trapping occurs first at the tail of the ion beam.

Forerunner electrons are generated via a dynamic and nonlinear process, which can be seen from the fact that the potential fluctuations become large and the electron dynamics

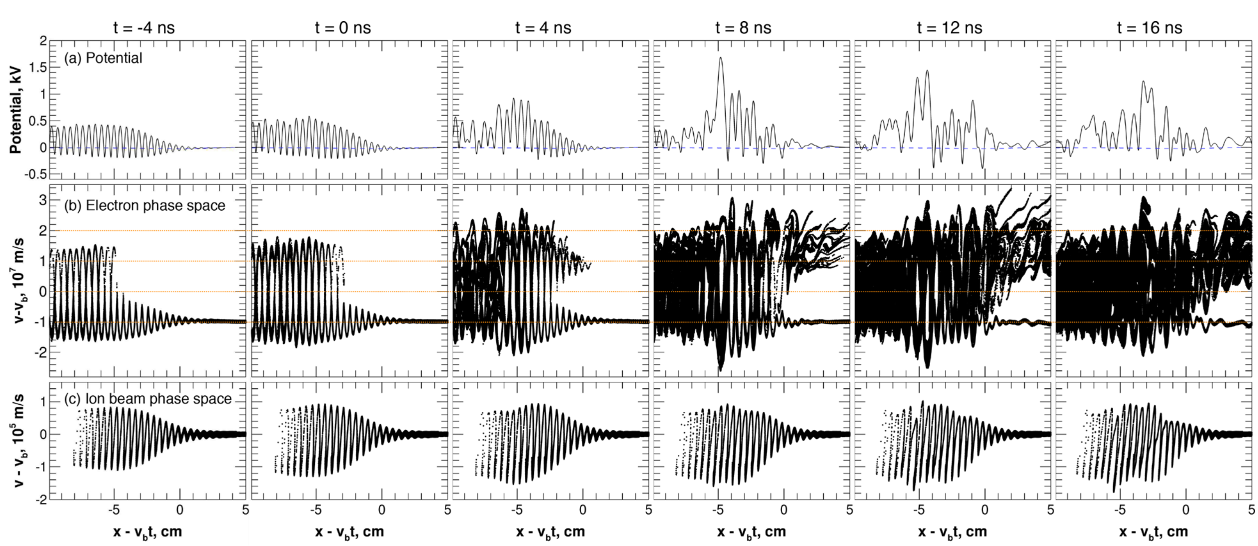

FIG. 1. Electron acceleration due to the two-stream instability caused by the neutralized ion beam in a 15 cm long window out of a 15 m long computational domain at different times. Shown are (a) the potential, (b) the electron phase space, and (c) the ion beam phase space at $-4\,\mathrm{ns} \leq t \leq 16$ ns. $t = 0$ ns is chosen to be the time when the forerunner electrons are generated, which is approximately 200 ns after the injection of the ion beam pulse into the plasma.

cannot be described by linear theory. This is also evident from Fig. 3 where electron detrapping occurs because the electric field is strongly modulated in time. Around $t \sim 0$ ns, the wave breaking causes the potential structure to become incoherent and nonstationary in the beam frame. At this time, electrons become detrapped, escape from the potential wells in the plasma wave, and are accelerated ahead of the beam pulse forming a forerunner electron beam. The formation of forerunner electrons becomes clear at $t = 4$ ns. The potential in the plasma wave becomes asymmetric and further grows to about 1.6 kV at maximum at $t = 8$ ns. After the electron acceleration occurs, the potential amplitude gradually decreases at $t > 8$ ns.

Additionally, the newly generated electron stream causes a secondary two-stream instability between the streaming electrons and the background plasma electrons (see Fig. 1; $x - v_b t > 2$ cm and $t \geq 8$ ns). This electron-electron instability growth rate $\gamma_s/\omega_{pe} \propto \sqrt[3]{n_s/n_p}$, where n_s is the density of the forerunner electron beam, is much faster than the initial ion-beam instability, e.g., ns-scale, because the secondary instability is between two electron populations. As shown in Fig. 2, the tip of the forerunner electron beam has a small thermal spread and the growth of the secondary electron-electron two-stream instability can be fast. For instance, $\gamma_s = 0.1\omega_{pe}$ even if $n_s = 10^{-3} n_p$, which results in a characteristic time of 5 ns. Therefore, this instability develops before the ion beam heating occurs on a time scale of 300 ns.

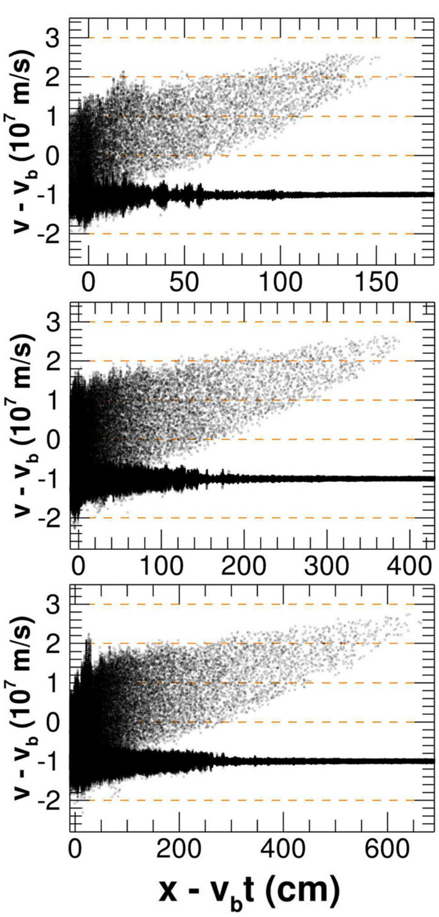

FIG. 2. Long time evolution of the electron phase space. Orange dashed lines are shown to help visualize the spread and propagation of the forerunner electrons.

B. Electron acceleration due to two-stream instability

As shown in Fig. 3, particles 2 (p2) and 3 (p3) are initially trapped by the plasma wave at the tail of the ion beam pulse ($x - v_b t < -5$ cm) for a few cycles. Because of the wave breaking at $t > 5$ ns, the electric field in the plasma wave becomes incoherent and accelerating and decelerating cycles of the electric field become asymmetric [see Fig. 3(b)], which causes the particles to escape trapping in the wave and accelerate to move faster than the ion beam. The resulting velocity of accelerated particles lies in the interval $v - v_b \in [0, 2v_b]$ (see Fig. 1); therefore, the generated forerunner beam travels faster than a mere reflection from potential well. Coherent plasma waves are observed near the ion beam pulse at $t > 18$ ns, long after the generation of a forerunner electron beam at $t \sim 0$ ns. These waves also experience modulation, which allows for the electron acceleration to occur even at later time and continuous generation of the forerunner electron beam.

The p1 trajectory is nearly symmetric around $v - v_b = 0$ in the phase space, which indicates that p1 is purely reflected by the time-varying large-amplitude plasma wave. As can be seen from the trajectory in the phase space, see Fig. 3(b), the p1 trajectory is not merely reflection from a potential hill. The mechanism of p1 acceleration in front of the ion beam is the same as for the p2 and p3 particles, while the only difference lies in fact that p1 is not fully *trapped* in the wave, i.e., it does not complete a full bounce motion in the trough of

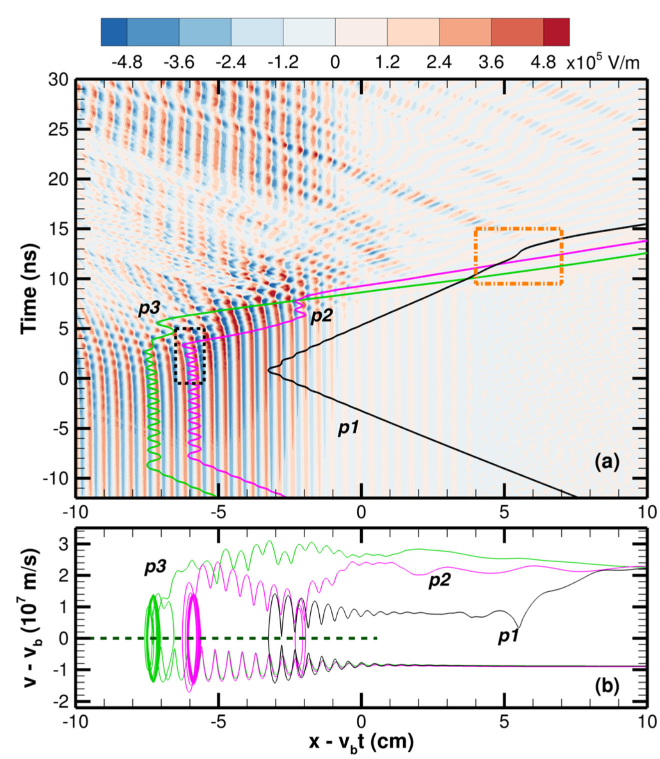

FIG. 3. Spatio-temporal evolution of the electric field and the trajectories of three test particles. Particle 1 (p1) is one of the first electrons that are reflected in front of the ion beam pulse. Particles 2 (p2) and 3 (p3) experience trapping and detrapping before being accelerated in front of the ion beam pulse.

the plasma wave, before being accelerated. For most forerunner electrons, the energy builds up by particle trapping and detrapping in the waves. Note that there are also particles that lose energy in this process, e.g., p2 at $x - v_b t = -2$ cm around $t = 5$ ns, see Fig. 3(a). After being reflected by the plasma wave, p1 is further accelerated at $x - v_b t = 5.5$ cm ($t = 13$ ns) in such a process as shown in Fig. 4(b). Once the detrapped particles, e.g., p2 and p3, form the forerunner beam, the electric field is modulated due to the secondary two-stream instability (see Fig. 1; $t > 8$ ns). This wave is responsible for additional acceleration of reflected particles, e.g., p1 from v_b to $(1\sim2)v_b$ in the beam frame, as shown in Figs. 3(b) and 4(b).

Details of electron acceleration are given in Fig. 4(a). It can be seen in Fig. 4(a) that the p2 electron gains energy and becomes accelerated forward by moving into a negative electric field, $E_{\min} = -560$ kV/m, shown by the purple triangle symbol in Fig. 4(a) at $x - v_b t = -6.26$ cm ($t = 3.3$ ns), which is considerably enhanced compared to the previous bounce period. After being accelerated, the electrons move through the region of a smaller decelerating field, $E_{\max} = 300$ kV/m, shown by the light blue square symbol in Fig. 4(a) at $x - v_b t = -5.83$ cm ($t = 3.8$ ns). This field is weaker than the accelerating field; therefore, the electrons become detrapped from the potential well and are being accelerated ahead of the beam pulse.

C. Saturation and decay of the instabilities

Figure 5 shows the temporal and spatial structures of the plasma wave at $30 \le t \le 300$ ns. From this figure, it is evident that the plasma wave amplitude remains relatively constant until the wave starts to decay at $t > 200$ ns. This enables the high-energy ion beam to transfer its energy into the plasma electrons for a long period of time.

The temporal evolution of the ion beam phase-space is shown in Figs. 6(a)–6(c) and the ion beam velocity distribution function (VDF) averaged over the entire beam pulse in Fig. 6(d). It can be seen from Figs. 6(a) and 6(b) that the ions are being trapped in the plasma wave within the first 200 ns (the minimum ion beam velocity reaches approximately $v - v_b = -3 \times 10^5$ m/s). The ion trapping occurs because there is a coherent plasma wave that is nearly stationary in the beam frame (see Fig. 5). At $t > 200$ ns, strong phase mixing leads to heating of the ion beam, as shown in Fig. 6(c). At that time, the plasma waves start decaying because of the thermalization of the ion beam.

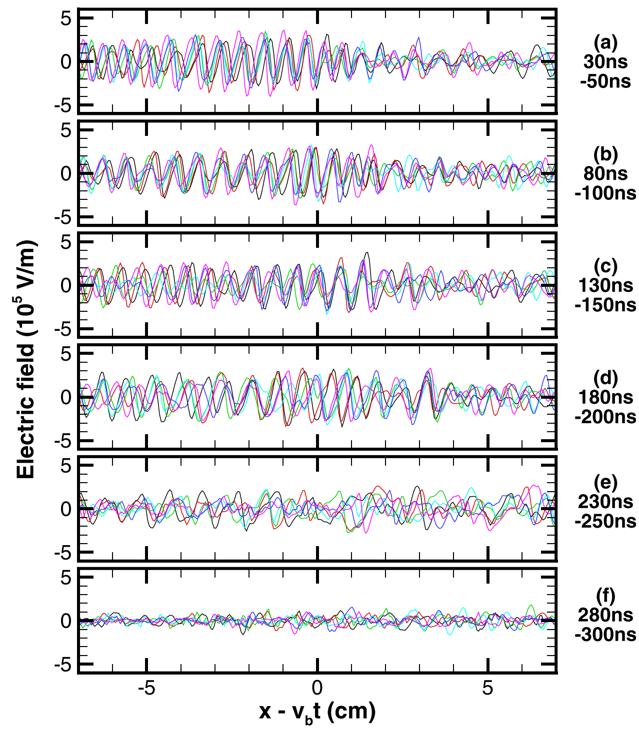

FIG. 5. Long-time evolution of plasma wave near the ion beam region at $-7\,\text{cm} < x - v_b t < 7\,\text{cm}$ after generation of forerunner electron beam. Six color lines (4 ns apart) are overlapped in each subfigures in the order of black, red, green, light blue, blue, and pink. Coherent plasma waves are observed at $x - v_b t < 3$ cm at $t \le 200$ ns. The wave in front of the ion beam is more chaotic.

Figure 6(d) shows that the mean velocity of the ion beam slows down because the ion beam energy is transferred to the electrons and plasma waves. For a sinusoidal periodic wave, the bounce frequency of the trapped beam ions in the plasma wave is given by $\omega_{B,i} = k(e\phi_{\max}/m_{i,b})^{1/2}$, where k is the wavenumber and $\phi_{\max}$ is the potential amplitude. Since $e\phi_{\max} \approx m_e v_b^2$ and $k \approx \omega_{pe}/v_b$ (see Ref. 18), the ion trapping time can be written as $\tau_{B,i} \equiv 2\pi/\omega_{B,i}$, where $\omega_{B,i} = (4\pi e^2 n_p/m_{i,b})^{1/2}$. This is independent of the ion beam velocity. Therefore, the increase in the ion beam velocity spread scales as $\Delta v_{i,b} = (2e\phi_{\max}/m_{i,b})^{1/2} \approx (2m_e/m_{i,b})^{1/2} v_b$, and the ion beam energy spread scales as $\Delta E_{i,b}/E_{i,b} \approx 2m_e/m_{i,b}$. From our simulation results, it follows that the ion beam trapping time $\tau_{B,i} \approx 200$ ns and $\Delta v_{i,b} \approx 10^5$ m/s, which are in agreement with the time required for nonlinear movement of beam ions in the plasma wave [see Fig. 5(e)]. We also observe that thermalization of the ion beam [see Fig. 6(d)] occurs on the same time scale.

Figure 7 shows the temporal evolution of the spatially averaged electron VDFs in the ion beam pulse region. The accelerated electron density increases before $t = 230$ ns and decreases after $t = 230$ ns, as can be seen from Figs. 7(b) to 7(c) due to wave decay after $t = 230$ ns. The electron

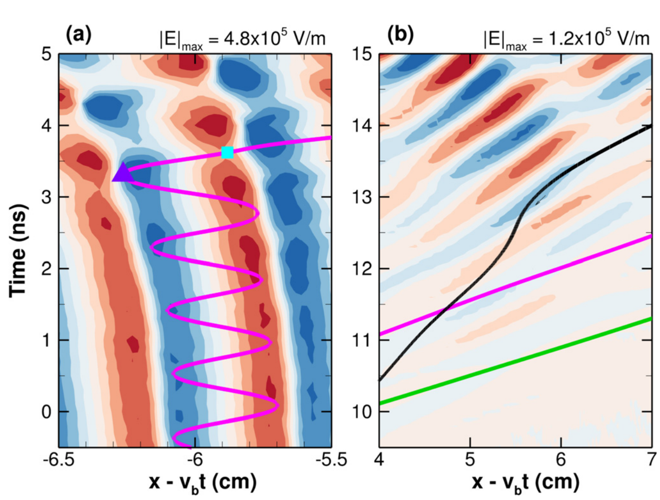

FIG. 4. Zoom-in of the black and orange boxes in Fig. 3(a), showing detrapping of p2 and additional acceleration of p1.

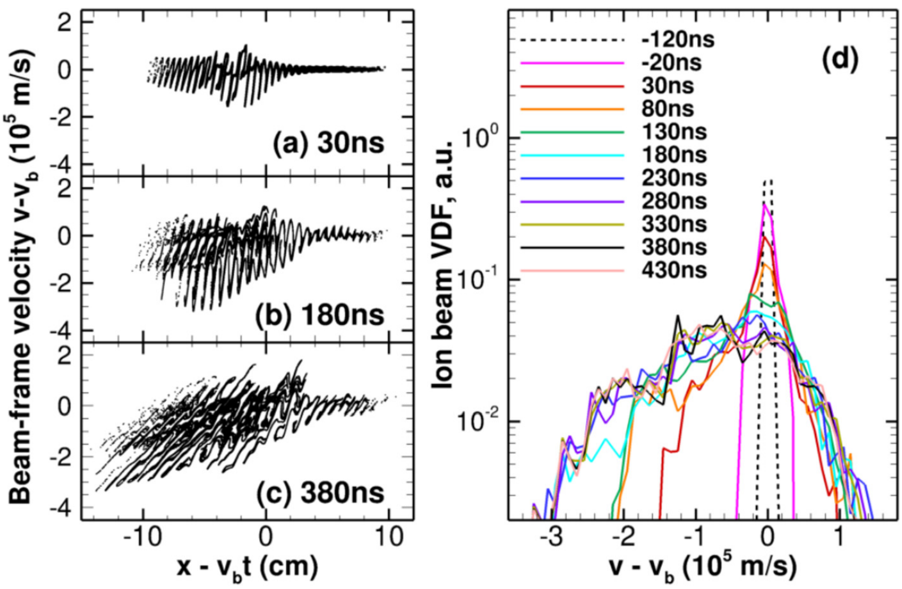

FIG. 6. Long-time evolution of ion beam in phase space at 30 ns (a), 180 ns (b), and 380 ns (c); and the averaged ion distribution for various time steps (d).

trapping time is given by $\tau_{B,e} = 2\pi/\omega_{B,e} \propto 2\pi/\omega_{pe}$, which is on the order of a nanosecond. In Fig. 7(a), heating of the background electrons (see $v \leq 0$ m/s) due to the secondary two-stream instability can also be observed up to $t = 230$ ns. Note that the position of the maximum of the VDF is shifted toward the negative velocity, while a significant amount of electrons is accelerated; thus, the total current is maintained, i.e., the current of the ion beam pulse is fully neutralized by the plasma electrons in the one-dimensional case. This may be different in a multidimensional setup if the beam radius is small compared to the skin depth, because the electron acceleration can occur along the beam axis and the return current may occur outside the beam.[38] Additionally, in the two-dimensional simulations in Ref. 38, the filamentation instability of the ion beam pulse was not observed during the time of the simulation. This is because the growth rate of the filamentation instability, γ_F, is much smaller than that of the two-stream instability, γ_T, for the nonrelativistic ion

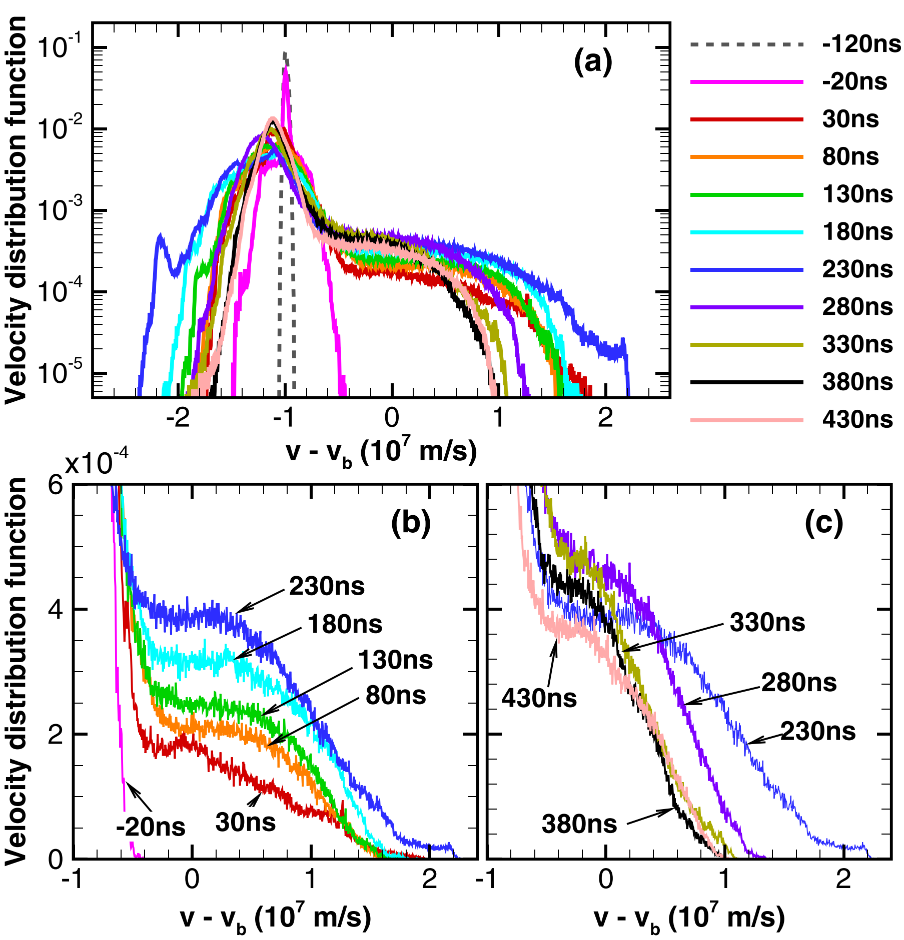

FIG. 7. Long-time evolution of electron VDFs that are spatially averaged in the ion beam pulse region, i.e., $-10\,\text{cm} < x - v_b t < 10\,\text{cm}$ for different times during ion beam propagation; (b) and (c) are zoom-in into the high velocity tail region.

beam. The ratio of the two growth rates[39] is $\gamma_F/\gamma_T \approx (n_b/n_p)^{1/6} v_b/c$ (for our simulation parameters $\gamma_F \approx 0.02\gamma_T \approx 1/320\,\mathrm{ns}^{-1}$). Therefore, the filamentation instability does not develop during simulation time of 320 ns.

IV. SUMMARY

We performed large spatial and long temporal studies of the two-stream instability produced by an ion beam pulse propagating in the background plasma using a one-dimensional electrostatic kinetic simulation. Examination of the electron trajectories forming the forerunner beam shows that the acceleration mostly occurs due to the energy gain during the electron trapping and detrapping in the nonstationary plasma wave setup after the initial saturation.

The strong plasma wave driven by the influx of the cold electrons from upstream persists for the time on the order of the bounce period of the beam ions ($\tau_{B,i} \propto 2\pi/(4\pi e^2 n_p/m_{i,b})^{1/2}$) and only decays when the beam ions become trapped and heated by the action of the wave. During this time, continuous generation of the forerunner electron beam was observed and the forerunner electron beam preheats the background plasma. The ion beam propagates over distance $v_b/\tau_{B,i}$ during the time $\tau_{B,i}$. Therefore, the strong defocusing forces caused by the two-stream instability[23,38] can affect the ballistic beam propagation in plasmas only on distances shorter than $v_b/\tau_{B,i}$. The ion beam heating due to the two-stream instability may cause longitudinal spread of the ion beam pulse and may affect the beam focusing in heavy ion fusion applications.

ACKNOWLEDGMENTS

The authors thank fruitful discussions with E. Tokluoglu, A. Khrabrov, and J. Carlson. Simulations were run on the supercomputing clusters at Princeton Plasma Physics Laboratory and Texas A&M University. This research was funded by the U.S. Department of Energy. K.H. acknowledges the Japan Society for the Promotion of Science (JSPS) for the postdoctoral fellowship.

[1]M. Roth, T. E. Cowan, M. H. Key, S. P. Hatchett, C. Brown, W. Fountain, J. Johnson, D. M. Pennington, R. A. Snavely, S. C. Wilks, K. Yasuike, H. Ruhl, F. Pegoraro, S. V. Bulanov, E. M. Campbell, M. D. Perry, and H. Powell, Phys. Rev. Lett. **86**, 436 (2001).
[2]C. Deutsch, Laser Part. Beams **22**, 115 (2004).
[3]A. Friedman, J. Barnard, R. Briggs, R. Davidson, M. Dorf, D. Grote, E. Henestroza, E. Lee, M. Leitner, B. Logan, A. Sefkow, W. Sharp, W. Waldron, D. Welch, and S. Yu, Nucl. Instrum. Methods, A **606**, 6 (2009).
[4]C. L. Olson, Nucl. Instrum. Methods, A **733**, 86 (2014).
[5]K. Papadopoulos, R. C. Davidson, J. M. Dawson, I. Haber, D. A. Hammer, N. A. Krall, and R. Shanny, Phys. Fluids **14**, 849 (1971).
[6]E. Mobius, K. Papadopoulos, and A. Pier, Planet. Space Sci. **35**(3), 345 (1987).
[7]P. J. Cargill and K. Papadopoulos, Astrophys. J. **329**, L29 (1988).
[8]M. E. Dieckmann, P. Ljung, A. Ynnerman, and K. G. McClements, Phys. Plasmas **7**, 5171 (2000).
[9]D. W. Forslund and C. R. Shonk, Phys. Rev. Lett. **25**, 1699 (1970).
[10]D. Montgomery and G. Joyce, J. Plasma Phys. **3**, 1 (1969).
[11]S. Iizuka, K. Saeki, N. Sato, and Y. Hatta, Phys. Rev. Lett. **43**, 1404 (1979).
[12]T. Sato and H. Okuda, Phys. Rev. Lett. **44**, 740 (1980).
[13]M. D. Campanell, A. V. Khrabrov, and I. D. Kaganovich, Phys. Rev. Lett. **108**, 235001 (2012).
[14]P. Seidl, A. Anders, F. Bieniosek, J. Barnard, J. Calanog, A. Chen, R. Cohen, J. Coleman, M. Dorf, E. Gilson, D. Grote, J. Jung, M. Leitner, S. Lidia, B. Logan, P. Ni, P. Roy, K. V. den Bogert, W. Waldron, and D. Welch, Nucl. Instrum. Methods, A **606**, 75 (2009).
[15]P. A. Seidl, A. Persaud, W. L. Waldron, J. J. Barnard, R. C. Davidson, A. Friedman, E. P. Gilson, W. G. Greenway, D. P. Grote, I. D. Kaganovich, S. M. Lidia, M. Stettler, J. H. Takakuwa, and T. Schenkel, Nucl. Instrum. Methods, A **800**, 98 (2015).
[16]S. Busold, D. Schumacher, C. Brabetz, D. Jahn, F. Kroll, O. Deppert, U. Schramm, T. E. Cowan, A. bel Blazevic, V. Bagnoud, and M. Roth, Sci. Rep. **5**, 12459 (2015).
[17]R. C. Davidson and H. Qin, Phys. Lett. A **270**, 177 (2000).
[18]I. D. Kaganovich, E. A. Startsev, and R. C. Davidson, Phys. Plasmas **11**, 3546 (2004).
[19]I. D. Kaganovich, E. A. Startsev, A. B. Sefkow, and R. C. Davidson, Phys. Rev. Lett. **99**, 235002 (2007).
[20]I. D. Kaganovich, E. A. Startsev, A. B. Sefkow, and R. C. Davidson, Phys. Plasmas **15**, 103108 (2008).
[21]W. Berdanier, P. K. Roy, and I. D. Kaganovich, Phys. Plasmas **22**, 013104 (2015).
[22]P. K. Roy, S. S. Yu, E. Henestroza, A. Anders, F. M. Bieniosek, J. Coleman, S. Eylon, W. G. Greenway, M. Leitner, B. G. Logan, W. L. Waldron, D. R. Welch, C. Thoma, A. B. Sefkow, E. P. Gilson, P. C. Efthimion, and R. C. Davidson, Phys. Rev. Lett. **95**, 234801 (2005).
[23]E. A. Startsev, I. D. Kaganovich, and R. C. Davidson, Nucl. Instrum. Methods, A **733**, 80 (2014).
[24]R. N. Sudan, Phys. Rev. Lett. **37**, 1613 (1976).
[25]M. A. Dorf, I. D. Kaganovich, E. A. Startsev, and R. C. Davidson, Phys. Rev. Lett. **103**, 075003 (2009).
[26]J. M. Mitrani, I. D. Kaganovich, and R. C. Davidson, Nucl. Instrum. Methods, A **733**, 65 (2014).
[27]E. Tokluoglu and I. D. Kaganovich, Phys. Plasmas **22**, 040701 (2015).
[28]M. E. Dieckmann, P. K. Shukla, and B. Eliasson, New J. Phys. **8**, 225 (2006).
[29]N. Hershkowitz, J. Geophys. Res. **86**(A5), 3307, https://doi.org/10.1029/JA086iA05p03307 (1981).
[30]S. Brunner, R. L. Berger, B. I. Cohen, L. Hausammann, and E. J. Valeo, Phys. Plasmas **21**, 102104 (2014).
[31]J. Park, D. Caprioli, and A. Spitkovsky, Phys. Rev. Lett. **114**, 085003 (2015).
[32]C. K. Birdsall and A. B. Langdon, *Plasma Physics via Computer Simulation* (Institute of Physics, 2005).
[33]T. E. Cowan, J. Fuchs, H. Ruhl, A. Kemp, P. Audebert, M. Roth, R. Stephens, I. Barton, A. Blazevic, E. Brambrink, J. Cobble, J. Fernández, J.-C. Gauthier, M. Geissel, M. Hegelich, J. Kaae, S. Karsch, G. P. Le Sage, S. Letzring, M. Manclossi, S. Meyroneinc, A. Newkirk, H. Pepin, and N. Renard-LeGalloudec, Phys. Rev. Lett. **92**, 204801 (2004).
[34]A. Stockem, F. Fiuza, A. Bret, R. A. Fonseca, and L. O. Silva, Sci. Rep. **4**, 3934 (2014).
[35]K. Hara, T. Chapman, J. W. Banks, S. Brunner, I. Joseph, R. L. Berger, and I. D. Boyd, Phys. Plasmas **22**, 022104 (2015).
[36]K. Hara, I. Barth, E. Kaminski, I. Y. Dodin, and N. J. Fisch, Phys. Rev. E **95**, 053212 (2017).
[37]O. Buneman, Phys. Rev. **115**, 503 (1959).
[38]E. Tokluoglu, I. D. Kaganovich, J. Carlsson, K. Hara, and E. A. Startsev, e-print arXiv:1711.09951.
[39]A. Bret, L. Gremillet, and M. E. Dieckmann, Phys. Plasmas **17**, 120501 (2010).